SPECTRAL DEPENDENCE OF THE BROAD EMISSION-LINE REGION IN AGN

Amri Wandel

Racah Institute of Physics, The Hebrew University of Jerusalem 91904, Israel

ABSTRACT

We derive a theoretical relation between R_{BLR}, the size of the broad-emission-line region of active galactic nuclei, and the observed soft X-ray luminosity and spectrum. We show that in addition to the well known $R_{BLR} \sim L^{1/2}$ scaling, R_{BLR} should depend also on the soft X-ray spectral slope and derive the expected relation between R_{BLR} and the X-ray luminosity and spectral index. Applying this relation to calculate a predicted BLR radius for ten AGN with reverberation data, we show that including the dependence on the spectrum improves the agreement between the calculated BLR radius and the radius independently determined from reverberation mapping. Similarly we evaluate an expression for the line width, and show that including the dependence on the spectrum significantly improves the agreement between the calculated BLR velocity dispersion and the observed FWHM of the Hβ line. The theoretical expression for the line width also provids a physical explanation to the anti-correlation between the soft X-ray slope and the emission-line width observed in narrow-line Seyfert galaxies.

Subject headings: galaxies: active — galaxies: nuclei — galaxies: Seyfert — quasars: emission-lines —X-rays: galaxies

1. INTRODUCTION

Recent results from reverberation-mapping of the broad emission-line regions (BLR) in AGN indicate that the BLR distance from the central radiation source roughly scales as $r \propto L^{1/2}$ (Koratkar & Gaskell 1991;Kaspi et.al. 1996; Peterson 1995). Our model provides a physical explanation to this scaling, and predicts an additional testable dependence on the spectral shape.

Most workers today agree that the line width in AGN is induced by Keplerian bulk motions. If this is the case, the BLR distance is directly related to the line width, and studying such relations could provide more observational input. Such an input seems to be found in a new class of Narrow-Line X-ray Galaxies (NLXG), which are similar to Seyfert 1 galaxies except for having relatively narrow permitted lines (FWHM $H_\beta <$ 2000km/sec) , and often stronger FeII emission (e.g. Walter and Fink 1993). Many NLXG show steep soft X-ray spectra, $\alpha_x >$ 2, while ordinary (broad line) AGN such as Seyfert 1's and quasars usually have $\alpha_x \sim 0.5 - 1.5$. Mixed samples (NLXG and ordinary AGN) show a strong correlation between the Hβ line width and the soft X-ray spectral index (Boller, Brandt and Fink 1996; Wang, Brinkmann and Bergeron 1996, hereafter WBB). The latter authors found the soft X-ray spectral index is correlated also with the FeII/Hβ ratio, and with the Hβ equivalent width.

We derive simple analytic relations between soft X-ray continuum spectrum (luminosity and spectral index) and the BLR size and the width of the broad emission lines, which explain the observed correlation between the X-ray slope and the line width (section 2). Applying the model to samples of AGN it gives a good agreement with the BLR sizes determined by reverberation mapping, and with the observed FWHM(Hβ) - cf. Wandel and Boller 1997b (section 3). Finally, in section 4 we suggest explanations of two additional empirical correlations (related to the Hβ equivalent width and the FeII emission) and discuss the validity of our basic assumptions.

2. THE MODEL

While there is probably a range of physical conditions (ionization parameter and density etc.) in the broad Hbeta line-emitting gas in AGNs, the emission of each line is dominated by emission in a relatively narrow optimum range of conditions (Baldwin et al. 1995). We will therefore make the assumption that the conditions relevant for Hβ can be approximated by a single value. We show that within the observational constraints on the far UV and soft X-ray bands of AGN spectra, the BLR size and the line width predicted by the model are not very sensitive to the detailed shape of the spectrum in the EUV band. We then estimate the BLR size, and assuming Keplerian velocity dispersion we relate it to the line width. The new element in our scheme is the use of the soft X-ray spectral index and luminosity to estimate the ionizing spectrum. The spectral index enters in the model as follows: a softer (that is steeper) spectrum has a stronger ionizing power, and hence the BLR is formed at a larger distance from the central source, has a smaller velocity dispersion and produces narrower emission lines. We parametrize the form of the ionizing EUV continuum in terms of the the break between the UV and X-ray bands and the measured soft X-ray slope α_x.

2.1. The BLR radius

We assume that the spatial extent of the BLR may be represented by a characteristic size - e.g. the radius at which the emission peaks.

The physical conditions in the line-emitting gas are largely determined by the ionization parameter (the ratio of ionizing photon density to the electron density, n_e, e.g. Netzer, 1990) $U = Q_{ion}/4\pi R^2 c n_e$ where the ionizing photon flux (number of ionizing photons per unit time) is $Q_{ion} = \int_{E_0}^{\infty} F(E)\frac{dE}{E}$, $F(E)$ is the luminosity per unit energy, and E_0 =1 Rydberg=13.6 eV. Defining the ionizing luminosity, $L_{ion} = \int_{E_0}^{\infty} F(E)dE$ and the mean energy of an ionizing photon, $\bar{E}_{ion} \equiv L_{ion}/Q_{ion}$, the BLR radius (expressed in light-days) may be written as

$$R = \left(\frac{L_{ion}}{4\pi c \bar{E}_{ion} U n_e}\right)^{1/2} = 13.4 \left(\frac{L_{x44}}{U n_{10} \epsilon_x}\right)^{1/2} \text{ ld} \tag{1}$$

where $n_{10} = n_e/10^{10} \quad cm^{-3}$, $L_{x44} = L_x/10^{44}$ ergs/sec is the observed X-ray luminosity, $\epsilon = \bar{E}_{ion}/E_0$ is the mean photon energy in Rydbergs, and $\epsilon_x = \epsilon L_x/L_{ion} = L_x/E_0 Q_{ion}$. Typical values in the gas emitting the high excitation broad lines are $U \sim 0.1 - 1$ and $n_e \sim 10^{10} - 10^{11} cm^{-3}$ (e.g. Rees, Netzer and Ferland, 1989), so that $U n_{10} \sim 0.1 - 10$. For L_x we consider two practical cases: broad band luminosity, (for the ROSAT band) $L_x = \int_{0.1keV}^{2.4keV} F(E)dE$ and a monochromatic luminosity defined by $L_x = EF(E)$ at E=0.3keV. The two cases give quite different R_{BLR} vs. α_x curves, as shown in fig.1.

2.2. The ionizing spectrum

The ionizing flux is dominated by the EUV continuum in the 1-10 Rydberg regime, where most of the ionizing photons are emitted. Since the the continuum in this range cannot be observed directly, we try to estimate it by extrapolation from the nearest observable energy bands. The far UV spectrum has been observed beyond the Lyman limit, for about 100 quasars (Zheng et al, 1996), to wavelengths of 600Å , and for a handful luminous, high redshift quasars to wavelengths of 350Å. The average spectrum has a slope of $\alpha \sim 1$ in the 1000-2000Å band, and below 900Å it steepens to $\alpha \sim 2$. In the soft X-ray band the observed spectrum is often steeper than this (especially in NLXGs, see Hasinger *et al.* 1993; Walter and Fink, 1993, but compare Laor *et al.* 1997). This indicated there may be a break or a turnover at some intermediate energy E_b between 10 and 100eV (cf. Mathews and Ferland 1987). We assume that the soft X-ray spectrum can be extrapolated to lower energies down to some break energy E_b, and below the break we take E^{-2}. For the hard X-rays ($E > 2keV$) we use the "universal" $E^{-0.7}$ power law, observed in most AGN with a high energy cutoff at 100keV (since the ionizing photon flux is dominated by the continuum near 1 Ryd, the model is insensitive to the assumed hard X-ray spectrum). In summary, we approximate the ionizing continuum spectrum by a broken power law of the form

$$F(E) \propto \begin{cases} E^{-2} & E_0 < E < E_b; \\ E^{-\alpha_x} & E_b < E < E_h; \\ E^{-0.7} & E_h < E < E_{max}; \end{cases} \tag{2}$$

where the break energy $E_b \geq E_0$ is a free parameter, E_h is the break energy at the hard X-ray band, and E_{max} is the high energy cutoff. In the calculations below we take $E_b = 0.1keV$ and $E_h = 2keV$.

Fig. 1 shows how the calculated BLR size depends on the X-ray spectral index, on the shape of the EUV spectrum (parametrized by E_b) and on the normalization of the X-ray

luminosity (broad-band or monochromatic). While the dependence on α_x is strong (R_{BLR} increases by a factor of 100 when α_x increases from 0 to 4), the dependence on the EUV shape is quite weak; changing E_b in the relevant range (13.6-100eV) changes R_{BLR} by less than 30% (for $\alpha_x < 3$). As expected, we find that R_{BLR} is almost independent of the hard X-ray parameters - E_h and E_{max}.

2.3. Line width

Assuming that the line width is induced by Keplerian motion in the gravitational potential of the central mass, the velocity dispersion corresponding to the full width at half maximum of the emission lines is given by $v \approx \sqrt{GM/R}$ where M is the mass of the central black hole and r the distance of the broad line region from the central source. Eq. (1) gives

$$v \approx 1900 \left(\frac{Un_{10}\epsilon_x}{L_{x44}}\right)^{1/4} \left(\frac{M}{10^7 M_\odot}\right)^{1/2} \text{ km/s.} \quad (3)$$

In order to relate the unknown mass to the observed luminosity we assume that the central mass approximately scales with the luminosity (Dibai 1981; Joly *et al.* 1985; Wandel and Yahil 1985; Wandel and Mushotzky 1986). In terms of the Eddington ratio these authors find for large AGN samples $L/L_{Edd} \approx 0.01 - 0.1$. Within this distribution, bright objects tend to have slightly larger L/M ratios than faint ones (cf. Koratkar and Gaskell 1991) roughly $L/M \propto L^{1/4}$ or $M \propto L^{3/4}$. Combining this with the correlation between the optical and the X-ray luminosities $L_x \propto L_{opt}^{0.75\pm0.05}$ (Kriss 1988; Mushotzky and Wandel 1989) gives

$$M \approx 7 \times 10^7 L_{x44} \left(\frac{L/L_{Edd}}{0.01}\right)^{-1} M_\odot. \quad (4)$$

and with eqs. (2) and (3) the line-width may be related directly to the observed X-ray luminosity and spectral index:

$$v(FWHM) \approx 5000\ \eta \epsilon_x^{1/4}(\alpha_x) L_{x44}^{1/4} \text{ km/s} \quad (5)$$

where $\eta \equiv (Un_{10})^{1/4}(L/L_{Edd}/0.01)^{-1/2}$ combines all the unknown parameters; for the $Un_{10} \sim 0.1 - 10$ and $L/L_{Edd} \sim 0.01 - 0.1$ stated above we have $\eta \sim 0.2 - 2$.

3. COMPARISON WITH THE DATA

3.1. BLR radius

We have Compared the BLR size calculated from the model with the distance from the central source obtained by reverberation mapping of the Hβ line, for a sample of 10 AGN for which reverberation and X-ray data were available (fig 2 and table 1). As we discuss below, the agreement *actually improves* by taking the X-ray spectral slope into account.

In the model calculations we have used the spectral index from the power-law fit to the ROSAT 0.1-2.4 keV band and E_b=1Ryd, (with the exception of NGC 3783, for which we have used $\alpha_x = 1.5$, see Walter and Fink, 1992; note also that NGC 4151 has an extended emission, Warwick et.al. 1995). The horizontal error bars represent the combined error in the luminosity and in the spectral index. Allowing for the uncertainty in $Un_{10} \sim 0.1 - 1$ (represented by the dashed lines in fig. 2), the agreement is quite good: all the points lie well within these boundaries. In order to test the significance of our model, we have calculated the BLR radii *without* taking into account the spectral dependence (that is, assuming all objects have *the same* soft X-ray

spectral slope, which we set to the sample average, α_x=1.45). We find that the difference between BLR size (calculated using only the luminosity scaling) and the reverberation size is significantly larger when the spectral dependence is not taken into account for three objects (NGC4151, PG0844 and NGC 3783) shown as gray dots in fig 2. For the other objects the difference is small in both calculations.

In order to compare our model to the empirical $R \sim L_{opt}^{1/2}$ relation, we have calculated the BLR radius using eq. (1) with $L = L_{opt}$ and $\epsilon = 1$. We denote these three models by $R(L_x, \alpha_x)$, $R(L_x)$, and $R(L_{opt})$.

The statistical significance of each model is tested by the χ^2 statistic,

$$\chi^2 = \sum_i \frac{[\log(R_i(\mathrm{obs})) - \log(R_i(\mathrm{mod}))]^2}{\sigma_i^2(\mathrm{obs}) + \sigma_i^2(\mathrm{mod})}.$$

The variance of each object is taken as the sum of the squared standard deviations of the observed radius (the error in the reverberation determination) and the calculated radius (the errors in the involved observables - L_x, α_x or L_{opt}. The χ^2 values obtained for the three models are $\chi^2(L_x, \alpha_x) = 0.88$, $\chi^2(L_x) = 1.77$, and $\chi^2(L_{opt}) = 1.56$. The corresponding confidence levels p are given by $1 - p = \Gamma(\nu/2, \chi^2/2)$ where ν is the number of degrees of freedom (here taken as 9). For the three models we get $1-p$=0.0043, 0.0091 and 0.0077 respectively.

3.2. Line width-spectral index correlation

Equation (5) predicts an explicit relation between the velocity dispersion (associated with the line width), the X-ray luminosity and the spectral index, namely a surface in the $\alpha_x - v - L_x$ space. For a fixed value of L_x this gives a curve in the $v - \alpha_x$ plane. Figure 3 shows such curves of FWHM vs.α_x for several values of the luminosity, $L_x = 10^{42}$-10^{45}ergs/sec (cf. Wandel and Boller 1997). Overplotted are the data points - FWHM(Hβ) vs. α_x for a sample of AGN (see below). The model seems to reproduce the distribution of the data very well, and in particular it explains the observed anticorrelation between the Hβ line width and the soft X-ray spectral index.

3.3. Predicted vs. observed line width

In order to test the model prediction over the three dimensional $\alpha - v - L_x$ space we compare the observed line width to the value calculated with eq. (5) using the measured X-ray spectral index and luminosity for a sample consisting of 33 ordinary AGN from Walter and Fink (1993) combined with 32 NLXGs (Boller, Brandt and ,Fink 1996). As can be seen in fig. 4a, the agreement is very good, and most of the objects fall well within the uncertainty strip of log FWHM(obs)=log v(mod)±0.5. Fig. 4b shows the same comparison when the spectral information is not taken into account (but rather its sample average, $\alpha_x = 1.74$): the correlation is significantly weeker. The correlation coefficient between the observed and calculated line widths is $r = 0.533$ and 0.316 respectively. The t-test statistic for zero regression

$t = r\sqrt{(N-2)}/\sqrt{(1-r^2)}$ gives for the two cases $t = 3.60$ and 2.40 respectively, for which the confidence levels for zero correlation are $1 - p = 0.0004$ and 0.01 respectively, and the dependent confidence level (which measures the significance of the dependence on spectral index, after taking out the dependence on the luminosity) is $p = 1 - 0.0004/0.01 = 0.96$.

3.4. Equivalent width

One may try to understand also the other strong correlations found in the data in terms of our model. The Hβ equivalent width is anti-correlated with the FWHM (Gaskell 1985, WBB) and with the soft X-ray spectral index; AGN with a steep soft X-ray spectrum have a lower EW(Hβ) than flat- spectrum AGN. To see how our model can explain this, we recall that the equivalent width measures the fraction of the continuum flux reprocessed and emitted in the line. We have shown (fig. 1) that the BLR distance from the central source increases with the spectral index. If the emission-line clouds are not pressure confined, it is reasonable that their sizes do not change significantly with the BLR radius, hence if clouds are conserved, the solid angle covered by the clouds decreases with radius, which implies that the equivalent width decreases with increasing (steepening) spectral index, as observed.

The author thanks Th. Boller, A. Laor, D. Maoz and H. Netzer for useful discussions, M.I. for help with the statistical analyses and M. Gaskell for the careful refereeing.

REFERENCES

Baldwin, J.A. *et al.* 1995, ApJ, 455 , L118.

Boller, T., Brandt W.N. and Fink, H. 1996 A&A, 305, 53.

Dibai, E.A. 1981, Soviet Astronomy Letters, 7, 248.

Ferland, G., Netzer, H. 1979, ApJ, 229, 274.

Kriss, G.A. 1988, ApJ, 324, 809.

Joly, M., Collin-Souffrin, S., Masnou, J.L., and Nottale, L. 1985, A&A, 152, 282.

Hasinger, G., Burg, R., Giacconi, R., *et al.* 1993 A&A, 275, 1.

Kaspi, Sh., Smith, P.S., Maoz, D., Netzer, H. and Jannuzi, T.J. 1996, ApJ, 471, L75

Koratkar, A. P. & Gaskell, C. M. ApJ370, L61

Laor, A., Fiore, F., Elvis, M. and Wilkes, B. 1997, ApJ

Maoz, D., in "Reverberation Mapping of AGN" eds. P.M.Gondhalekar, K.Horne, B.M. Peterson, SFASP 1995.

Mathews, W.G. and Ferland, G.J. 1987, ApJ, 323 , 456.

Mushotzky, R.F. and Wandel, A. 1989, ApJ, 339, 674.

Netzer, H. 1990 in "Active Galactic Nuclei", Saas-Fee Advanced Course 20, eds. T.J.-L. Courvoisier and M. Major, Springer Verlag, Berlin, p. 57.

Peterson, B.M. in "Reverberation Mapping of AGN" eds. P.M. Gondhalekar, K.Horne, B.M.Peterson, SFASP 1995.

Rees, M., Netzer H., Ferland, G.J. 1989. ApJ, 347, 640.

Walter, R. and Fink, H.H. 1993, A&A, 274, 105.

Wandel, A. 1996, in "X-ray Imaging and Spectroscopy of Cosmic Hot Plasmas", p. 307, ed. F.Makino, K. Mitsuda, Universal Academy Press, Tokyo .

Wandel, A. and Boller, Th. 1997a, in "Time Sequences", ed. D. Maoz, Kluwer.

Wandel, A. and Boller, Th. 1997b, A&A, submitted.

Wandel, A. and Mushotzky, R.F. 1986, ApJ, 306, L61.

Wandel, A. and Yahil, A. 1985, ApJ, 295, L1.

Wang, T., Brinkmann, W., and Bergeron, J. 1996, (WBB) A&A, 309, 81.

Warwick, R. *et al.* 1995, MNRAS, 275, 1003.

Zheng, W., Kriss, G.A., Telfer, R.C., Grimes, J.P., and Davidsen, A.F., ApJ, 475, 469.

Figure Captions

Fig. 1.— The calculated BLR radius vs. the soft X-ray spectral index α. Shown are two assumed EUV spectra: (a) $E_b = 1$Ryd, so that $\alpha_{EUV} = \alpha_x$ (solid curves), and (b) $E_b = 100eV$, $\alpha_{EUV} = 2$ (dashed curves). For each case we show two luminosity normalizations: monochromatic - $L_x(0.3keV) = 10^{44}$ergs/sec (the *upper* two curves, indicated by 0.3keV) and the ROSAT band normalization (see text) - $L_x(0.1 - 2.4keV) = 10^{44}$ergs/sec (the *lower* two curves, indicated by 0.1-2.4keV).

Fig. 2.— The BLR size determined from reverberation mapping of the Hβ line vs. the radius calculated from the model (eq. (1)) using the observed X-ray luminosity and spectral index. The reverberation radii are from Kaspi et.al. (1996), and the X-ray data from Walter and Fink (1993) except NGC 4151 (Warwick *et al.* 1995) and PG 0026 and PG 0844 from WBB. The grey circles represent the radius calculated from the model without taking the spectral dependence into account (see text). The solid line represents $R_{rev} = R_{model}$ for $Un_{10} = 1$ while the dashed parallel lines above and below it correspond to $Un_{10} = 0.1$ and 10 respectively.

Fig. 3.— Theoretical curves of the X-ray spectral index vs. v(BLR) for fixed values of $L_x = 10^{42}$ergs/sec (lower curve) to $L_x = 10^{45}$ergs/sec (upper curve) superimposed on the data for the sample of NLXGs and normal Seyferts.

Fig. 4.— Observed FWHM(Hβ) vs. $v(L_x, \alpha_x)$ (the velocity dispersion calculated with the observed X-ray spectral index and luminosity, eq. (5)) - figure 4a, and FWHM(Hβ) vs. $v(L_x)$ (calculated with only the observed X-ray luminosity- figure 4b. The diagonal line represents the equality ($v = FWHM$) for $\eta = 0.6$, while the dashed parallel lines above and below the diagonal are for $\eta = 0.2$ and 2 respectively.

This 2-column preprint was prepared with the AAS LATEX macros v4.0.

Table 1

X-ray and Optical data, reverberation and model BLR radius.

Object	Name	Log L_X	Log L_{opt}	α_x	$R_{rev}(H\beta)^{a}$	$R(L_x,\alpha_x)^{b}$	$R(L_x)^{b}$	$R(L_{opt})^{b}$
1	NGC 3783	43.5±0.16	43.5±0.2	1.50±0.40	0.92±0.08	0.91±0.29	0.88±0.08	0.90±0.1
2	NGC 5548	44.0±0.06	43.8±0.2	1.21±0.15	1.23±0.10	1.00±0.11	1.13±0.03	1.05±0.1
3	MKN 279	44.26±0.07	44.2±0.1	1.15±0.17	1.00±0.10	1.10±0.13	1.26±0.035	1.24±0.05
4	AK 120	44.86±0.08	44.15±0.25	1.63±0.29	1.46±0.15	1.66±0.19	1.56±0.04	1.20±0.12
5	MKN 590	44.2±0.08	44.3±0.2	1.01±0.24	1.27±0.04	1.00±0.17	1.23±0.04	1.30±0.1
6	PG 0804	45.2±0.1	45.3±0.1	1.53±0.41	1.92±0.23	1.78±0.26	1.73±0.05	1.80±0.06
7	NGC 4541	43.1±0.1	43.2±0.2	1.80±0.1	0.85±0.25	0.87±0.10	0.68±0.05	0.74±0.1
8	PG 0953	45.16±0.05	45.7±0.2	1.31±0.28	1.95±0.20	1.64±0.17	1.71±0.025	1.98±0.1
9	PG 0844	43.7±0.08	45.4±0.3	1.82±0.95	1.57±0.27	1.17±0.50	0.98±0.04	1.83±0.15
10	NGC 3516	42.7±0.03	43.5±0.1	1.49±0.42	0.59±0.12	0.50±0.23	0.48±0.015	0.88±0.05

[a]Log of BLR radius from reverberation mapping in light days

[b]Log of BLR radius calculated from the model in light days (see text)

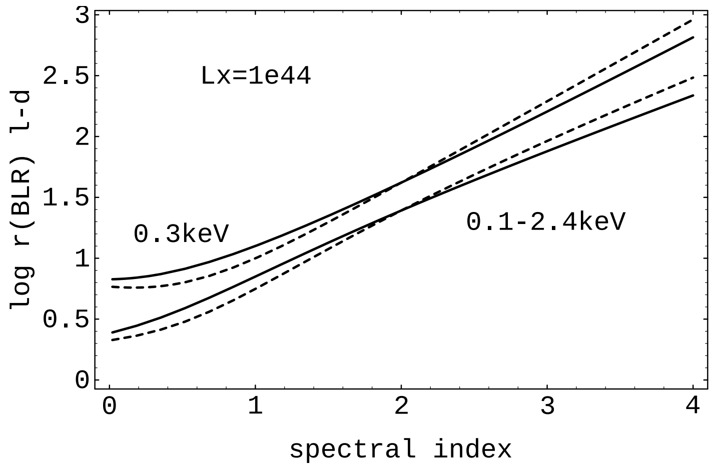

Lx=1e44
0.3keV
0.1-2.4keV
log r(BLR) l-d
spectral index
0
0.5
1
1.5
2
2.5
3
0
1
2
3
4

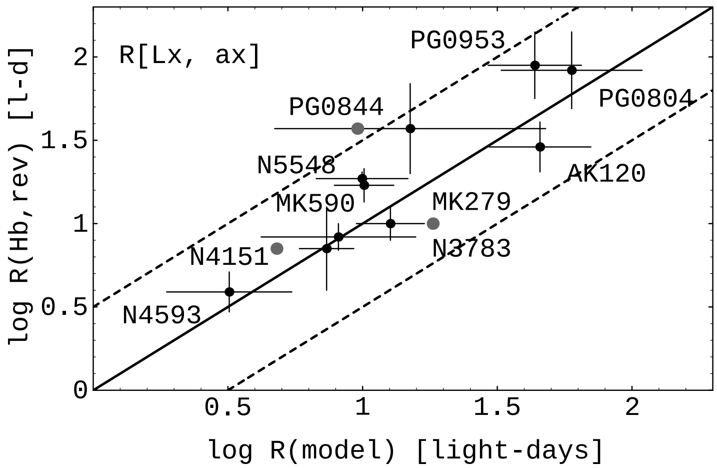
R[Lx, ax]
PG0953
PG0844
PG0804
N5548
AK120
MK590
MK279
N4151
N3783
N4593
log R(Hb,rev) [l-d]
log R(model) [light-days]
0
0.5
1
1.5
2
0.5
1
1.5
2

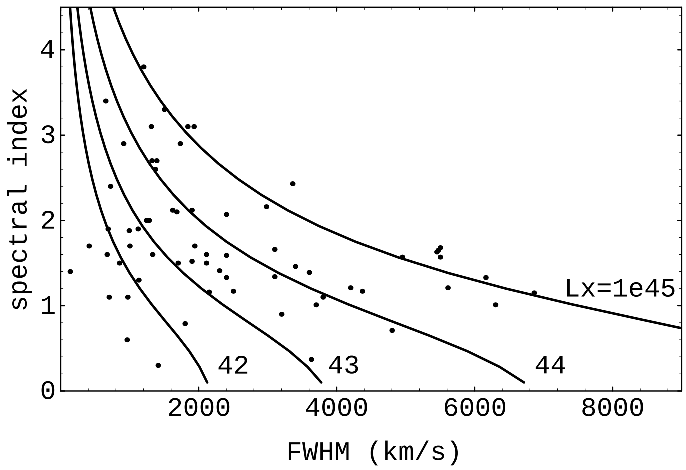

spectral index
FWHM (km/s)
Lx=1e45
42
43
44
0
1
2
3
4
2000
4000
6000
8000

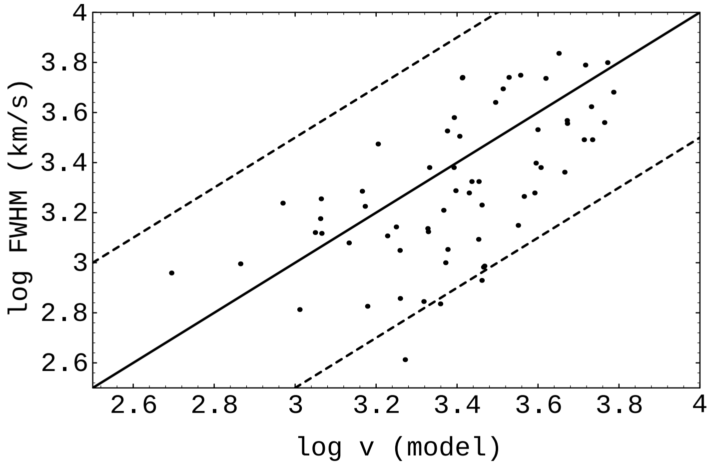

log FWHM (km/s)
log v (model)
4
3.8
3.6
3.4
3.2
3
2.8
2.6
2.6
2.8
3
3.2
3.4
3.6
3.8
4

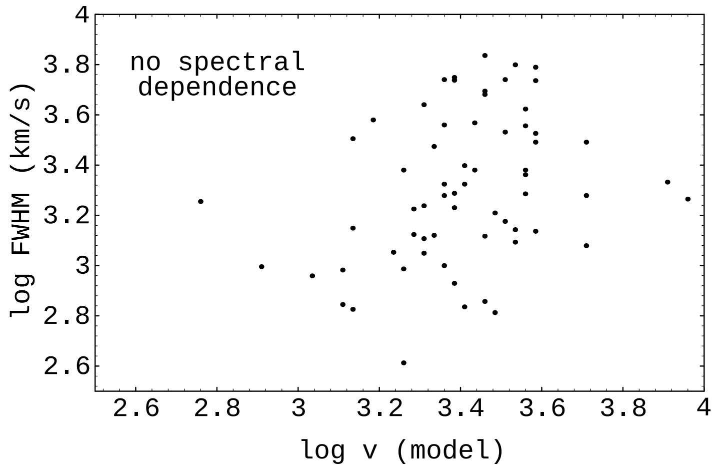
no spectral
dependence
log FWHM (km/s)
log v (model)
4
3.8
3.6
3.4
3.2
3
2.8
2.6
2.6
2.8
3
3.2
3.4
3.6
3.8
4